Climate Dynamics (2026) 64:51
https://doi.org/10.1007/s00382-025-08029-4

Ocean mixed-layer damping and air–sea coupling modulate multidecadal spectral selectivity in the North Atlantic

Hongyuan Zhao[1] · **Jianping Li**[1,2]

Received: 31 May 2025 / Accepted: 28 December 2025
© The Author(s), under exclusive licence to Springer-Verlag GmbH Germany, part of Springer Nature 2026

Abstract
The stochastic climate model successfully predicts the red spectrum characteristic in climate variability, yet it fails to account for the specific frequency preference such as the Atlantic Multidecadal Oscillation (AMO). This study reveals the mechanism of frequency-selective amplification driven by stochastic forcings. Using a linear feedback model, we demonstrate that the oceanic damping effect (modulated by mixed layer depth, wind speed and latent heat sensitivity) acts as a frequency filter, converting broadband stochastic atmospheric forcings into low-frequency responses. Extending to a two-dimensional system, we construct an oscillator driven by stochastic forcing, wherein specific low-frequency components are amplified through ocean–atmosphere coupling. Analytical solutions link the spectral peak to the dynamical parameters, which are determined by the system's coupling and feedback process. Applied to the North Atlantic, this framework explains (1) the multidecadal timescale preference via ocean damping effect and (2) North Atlantic Oscillation-AMO transitions through stochastically forced oscillation. By resolving dynamics between stochastic forcing and deterministic responses, our results advance understanding of the origins of climatic quasi-periodicity.

Keywords AMO · NAO · Multidecadal variability · Stochastic climate model · Spectral selectivity

1 Introduction

The Atlantic Multidecadal Oscillation (AMO) is characterized by basin-scale sea surface temperature (SST) anomalies with a quasi-periodicity of 60–80 years (Kerr 2000; Schlesinger and Ramankutty 1994). The physical origin of the AMO has long been debated. From the perspective of deterministic theory, the multidecadal variability comes from oceanic internal oscillations. Many explanations identify the driver of the AMO as the Atlantic Meridional Overturning Circulation (AMOC) (Zhang et al. 2016, 2019). The natural multidecadal variability of the AMOC involves feedbacks of the density effect of salinity on deep convection, surface salinity transport and the Arctic (Lozier et al. 2012; Wei et al. 2022).

The stochastic forcing is also suggested as the generation mechanism for decadal variability (Liu 2012). The stochastic climate theory (Hasselmann 1976; Frankignoul and Hasselmann 1977) describes the slow climate components as Brownian integrators of fast atmospheric noise. The cumulative integration of white noise forcing by high-inertia subsystems (e.g., ocean) generates a red spectrum. The AMO can emerge in slab-ocean models without the role of ocean circulation, suggesting that the AMO is the response to stochastic forcing from the mid-latitude atmospheric circulation (Clement et al. 2015; Cane et al. 2017). However, the assumptions of the stochastic model generally ignore the frequency selectivity of the system. Understanding the mechanisms underlying the preferred timescale is crucial for understanding the quasi-periodic properties of low-frequency climate variability (Pivotti and Anderson 2021). Furthermore, the deterministic and stochastic dynamics can also be combined in an integrated framework. It is suggested

✉ Jianping Li
ljp@ouc.edu.cn

[1] Frontiers Science Center for Deep Ocean Multi-Spheres and Earth System (DOMES)/Key Laboratory of Physical Oceanography/Academy of Future Ocean/College of Oceanic and Atmospheric Sciences/Center for Ocean Carbon Neutrality, Ocean University of China, Qingdao 266100, China

[2] Laboratory for Ocean Dynamics and Climate, Qingdao Marine Science and Technology Center, Qingdao 266237, China

Published online: 14 January 2026

that though the AMO is from the ocean's internal modes rather than being directly driven by the atmosphere, it still requires excitation by atmospheric noise (Frankcombe et al. 2009).

The atmosphere over the North Atlantic exhibits multidecadal variability, such as the North Atlantic Oscillation (NAO)—the dominant atmospheric dipole mode in this region, which is reported to have multidecadal spectrum peak (Li and Wang 2003; Sun et al. 2015; Zhao et al. 2024a, b). Treating the forcing as purely stochastic noise (Zhao et al. 2020; Clement et al. 2015) ignores the presence of such low-frequency signals in the atmosphere. Frankcombe et al. (2009) revealed that noise forcing with spatiotemporal coherence (e.g., mimicking the NAO) significantly amplifies the internal mode's amplitude. Some studies consider coupled atmosphere–ocean feedbacks. Observational and modeling studies reveal a delayed response: the NAO forces AMOC adjustments through wind-driven transport and heat fluxes (Delworth and Greatbatch 2000; Eden and Jung 2001; Álvarez-García et al. 2008), influencing AMO phases with a 15–20 year lag (Delworth et al. 2017; Li et al. 2013). Then the AMO modulates the multidecadal variability of the NAO through its conversion to the North Atlantic Tripole (NAT) mode (Sun et al. 2015; Álvarez-García et al. 2008) and stratosphere-troposphere coupling (Omrani et al. 2022), exerting delayed negative feedback on the NAO with a lag of 15–20 years. A multidecadal loop is constructed by Sun et al. (2015):$\cdots \rightarrow \mathrm{NAO}^{+}$ (positive NAO phase) $\rightarrow \mathrm{AMO}^{+} \rightarrow \mathrm{NAO}^{-} \rightarrow \mathrm{AMO}^{-} \cdots$. While empirical models successfully replicate this delayed oscillator behavior through parameter tuning, the observed 15–20 year delay and spectra peak lacks explicit linkage to the inherent properties of the ocean or the air–sea coupling process strength.

In this paper, we describe a mechanistic framework to resolve the limitations above. Through observation data and simplified models, we analyze how the frequency selectivity (the preferred timescale) is shaped by intrinsic dynamics of the air-sea system in the North Atlantic. Section 2 gives the data and methods used in this paper. Section 3 analyses the filtered SST response at low frequency in the linear feedback stochastic model and its regional specificity. In Sect. 4, we constructed an air-sea coupled model with stochastic forcing and linear feedback. The spectrum character of the model is analyzed and we applied it to the NAO-AMO coupled oscillation. Section 5 gives the summary and discussion.

2 Data and methods

2.1 Data and index definition

The sea level pressure (SLP) data is from the HadSLP2 dataset (Allan and Ansell 2006). The SST data is from the Extended Reconstructed SST Version 5 dataset (Huang et al. 2017). The mixed layer depth is from the NCEP Global Ocean Data Assimilation System (GODAS) dataset (Derber and Rosati 1989). The mixed layer depth is defined as the depth where the temperature difference from the SST is less than 0.8 K. The 10 m wind data is from the NCEP-NCAR Reanalysis 1 dataset (Kalnay et al. 1996). The AMO index (AMOI) is defined as the area-weighted average of the detrended SST anomaly in the North Atlantic domain (75°–7.5°W, 0°–60°N). The NAO index (NAOI) is defined as the difference between the normalized SLP zonally averaged from 80°W to 30°E at 35°N and 65°N (Li and Wang 2003).

2.2 Linear damping model and estimation of the SST damping coefficient

The linear feedback model with stochastic noise is:

$$\frac{dy}{dt} = \alpha\xi\left(t\right) - \lambda y, \tag{1}$$

where y is the model response, $\xi\left(t\right)$ is the input forcing, set as white noise, α is the amplitude coefficient and $\lambda = \frac{1}{\beta}$ is the linear damping coefficient. A positive (negative) λ indicates a negative (positive) feedback effect.

When considering y as the SST anomalies, we calculated the damping coefficient based on the classical parameterization scheme of turbulent heat flux. Here are the bulk transfer formulas of the surface sensible heat flux (Q_{SH}) and latent heat flux (Q_{LH}).

$$Q_{SH} = \rho^{a} C_{p}^{a} C_{S} \left|\overrightarrow{U}\right| \left(T_{s} - T_{a}\right)$$

$$Q_{LH} = \rho^{a} L C_{L} \left|\overrightarrow{U}\right| \left(q_{s} - q_{a}\right)$$

where T_s is the SST, T_a is the air temperature, q_s is the saturation specific humidity at SST, and q_a is the air specific humidity. The ocean damping coefficient of sensible heat flux λ_{SH} is calculated following Frankignoul and Hasselmann (1977):

$$\lambda_{SH} = \frac{1}{\rho^{w} C_{p}^{w} h} \frac{\partial Q_{SH}}{\partial T_{s}} = \frac{\rho^{a} C_{p}^{a} C_{S} \left|\overrightarrow{U}\right|}{\rho^{w} C_{p}^{w} h},$$

where h is the mixed layer depth (m), and $\overrightarrow{U}$ is the 10 m wind speed (m s^{-1}). The other constant variables are shown in Table 1.

Following Frankignoul and Hasselmann (1977) and Frankignoul et al. (1998), the ocean damping coefficient of latent heat flux λ_{LH} is estimated from

$$\lambda_{LH} = \frac{1}{\rho^w C_p^w h}\frac{\partial Q_{LH}}{\partial T_s} = \frac{\rho^a L C_L \left|\overrightarrow{U}\right|}{\rho^w C_p^w h}\frac{\partial q_s}{\partial T_s} = \frac{\rho^a L C_L \left|\overrightarrow{U}\right|}{\rho^w C_p^w h}\frac{q_s L}{R_v T_s^2}.$$

Therefore, the damping caused by turbulent heat flux is the sum of sensible heat damping and latent heat damping.

$$\lambda_{turb} = \lambda_{SH} + \lambda_{LH} = \frac{\rho^a |\vec{U}|}{\rho^w C_p^w h}\left(C_p^a C_S + \frac{C_L q_s L^2}{R_v T_s^2}\right). \quad (2)$$

where the unit of λ_{turb} calculated from the raw data is s^{-1}. In the subsequent analysis, when reporting the λ value, we converted the unit to $year^{-1}$ for clarity. We use the annual climatology of wind speed, mixed layer depth and SLP from the raw monthly data in 1980–2015 to calculate the λ.

2.3 Numerical integration of stochastic differential equations

Both the linear feedback and the two-component coupling model used in this paper contain stochastic terms driven by Wiener processes. The stochastic differential equations were integrated using the Euler–Maruyama scheme (Higham 2001), where deterministic terms are advanced with a time step Δt, and stochastic increments are generated as independent Gaussian variables with zero mean and variance Δt. Specifically, the temporal differential of a variable X is:

$$dX = f_1(X,t)\,dt + f_2(X,t)\,dW(t),$$

Table 1 Constant variables used in the parameterization

Symbol	Description	Value
ρ^w	Density of seawater	1025 kg m^{-3}
C_p^w	Specific heat of seawater at constant pressure	4020 J kg^{-1} K^{-1}
ρ^a	Density of air	1.29 kg m^{-3}
C_p^a	Specific heat of air at constant pressure	1004 J kg^{-1} K^{-1}
C_S	Bulk transfer coefficient for sensible heat flux	1.0 * 10^{-3}
C_L	Bulk transfer coefficient for latent heat flux	1.35 * 10^{-3}
L	Latent heat of evaporation	2.5 * 10^6 J kg^{-1}
R_v	Specific gas constant for water vapor	461 J kg^{-1} K^{-1}

where $f_1(X,t)\,dt$ is the deterministic term and $f_2(X,t)\,dW(t)$ is the stochastic term. $W(t)$ is the standard Wiener process and $dW(t) \sim N(0, dt)$. The discrete numerical equation is:

$$X_{n+1} = X_n + f_1(X_n, t_n)\,\Delta t + f_2(X_n, t_n)\,\Delta W_n$$

where Δt is the time step and $\Delta W_n = W(t_{n+1}) - W(t_n) \sim N(0, \Delta t)$. The Wiener increments ΔW_n are assumed independent between time steps.

3 Spectral selectivity in the linear damping model

From Hasselmann (1976), the power spectrum density (PSD) of response y of Eq. (1) is

$$G(\omega) = \frac{F(\omega)}{\omega^2 + \frac{1}{\beta^2}}, \quad (3)$$

where $F(\omega)$ is the spectrum of the forcing and ω is the angular frequency. From this equation,$\beta = \frac{1}{\lambda}$ determines the frequency response of y to the forcing. This response function describes the behavior of a low-pass filter. Here, the half-power point $\omega_c = \frac{1}{\beta}$ is defined as the cutoff frequency of this low-pass frequency band. For frequencies lower (higher) than ω_c, the system amplifies and maintains (attenuates and smoothens) them.

Figure 1a and b show an example of $\beta = 5$ to demonstrate the spectral characteristics. Figure 1a gives the spectrum of the input with ideal flat power and the corresponding response $G(\omega)$. The response power is amplified at low frequencies and attenuated at high frequencies. We further calculate a numerical example with an integration time of T=5000 (dimensionless time unit) and a time step size $\Delta t = 0.1$. Figure 1b shows the spectrum of the artificial white noise (random numbers of a normal distribution) and the corresponding response. Notably, the white noise with finite length exhibits non-flat spectral characteristics. For a single realization, the model amplifies the subtle spectral structures in the input, converting broadband forcing into a response with spectral peaks. This indicates that the low frequency response arises from both theoretical response function and the weak spectral peak in the forcing. Figure 1c give the response PSD under different time scales. The cutoff frequency decreases as β increases, and the corresponding low-frequency response also strengthens. This demonstrates the strong control effect of β on the spectral characteristics of the response.

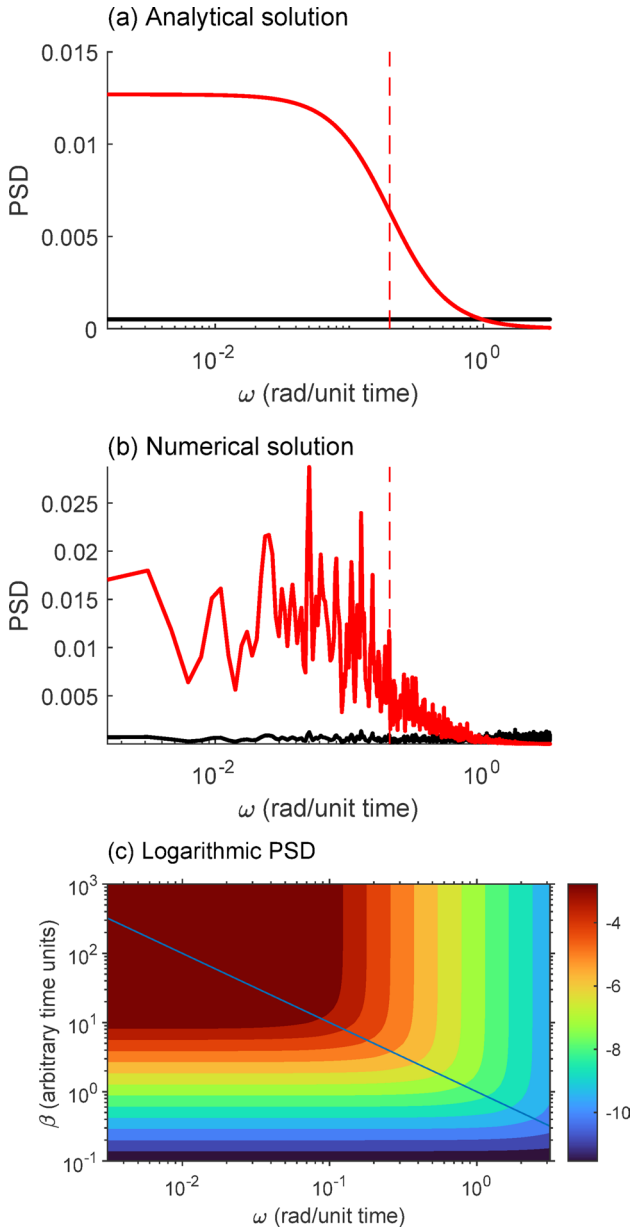

Fig. 1 Spectral characteristics of noise-driven responses in the linear feedback model. **a** Spectrum of ideal white noise (black solid line) and the analytical response spectrum from the linear feedback model (red solid line). **b** Spectrum of artificially generated white noise forcing (black solid line) and its response from the linear feedback model (red solid line). The red dashed lines in **a** and **b** indicate the $\omega_c = \frac{1}{\beta}$. The PSD was computed by Fourier-transforming the sample autocorrelation and the maximum lag $m = n/5$ (n is the number of data points). **c** Spectrum of the response to artificially generated white noise forcing from the linear feedback model for β values ranging from 10^{-1} to 10^{3}. The values of the power spectrum have been logarithmically processed. The power spectrum is plotted on a logarithmic scale (base 10). The blue solid line indicates the $\omega_c = 1/\beta$

The linear feedback model response $G(\omega)$ reveals that the amplified frequency band is controlled by the damping coefficient λ. Here, we further analyze the spatial heterogeneity of the timescale of SST variability by estimating the λ value of ocean. The damping term λ in the SST tendency equation represents the collective dissipation of thermal anomalies through air-sea heat fluxes, radiative cooling and oceanic dynamics (Frankignoul 1985; Gunnarson et al. 2024). Here, we calculated the turbulent heat flux damping coefficient (sum of latent and sensible damping) using the parameterization scheme (Eq. 2) of Frankignoul and Hasselmann (1977) and Frankignoul et al. (1998), as detailed in Sect. 2.2.

Figure 2a gives the λ_{turb} using the parametrization. For comparison, we also calculated the linear damping coefficient using the autocorrelation of the grid-point SST series ($\lambda = -ln\frac{\rho_1}{\Delta t}$, where ρ_1 is the lag-1 autocorrelation and $\Delta t = 1year$) in Fig. 2b. The λ values obtained by both methods show high-value areas at subpolar regions (subpolar North Atlantic and Southern Ocean) and low-value areas at low latitudes (Pacific cold tongue and). The cutoff period, given by $T_c = \frac{2\pi}{\lambda_{turb}} = 2\pi\beta$, is shown in Fig. 2c. It corresponds to the lower period limit of the low-pass response. This period represents the typical time scale of climate fluctuations that can be effectively maintained by the thermal inertia of the ocean mixed layer and the turbulent damping. In regions with lower λ values, such as the subpolar North Atlantic, sub-polar North Pacific and Southern Ocean, the corresponding T_c at the half-power point is longer. The T_c in the subpolar North Atlantic is particularly long with a value of 50 years, suggesting that it acts as a filter, favoring the multidecadal variability.

To compare the T_c with the characteristic timescale of SST, we use a Gaussian lowpass filter with an 11-year window to extract the decadal variance of SST at each grid point (Fig. 2d). The decadal variance in the subpolar regions is also large, especially in the North Atlantic Ocean, where the AMO, an important multidecadal mode in the ocean, is located. These results reveal that the ocean damping coefficient helps explain the timescale of SST variability.

To further investigate the dominant influencing factors of the spatial distribution of λ_{turb}, we examined the variables with spatial heterogeneity in parameterization (Fig. 3). The maximum values of mixed layer depth are observed in the North Atlantic, North Pacific, and Southern Ocean (Fig. 3a) and is highly similar to the distribution of T_c. This implies that the subpolar regions have a higher heat capacity, which influences the time scale of variability. The 10 m wind speed is lower in the subpolar North Atlantic and North Pacific (Fig. 3b), thus limiting the intensity of turbulent heat flux. Due to the nonlinear variation of saturated vapor pressure

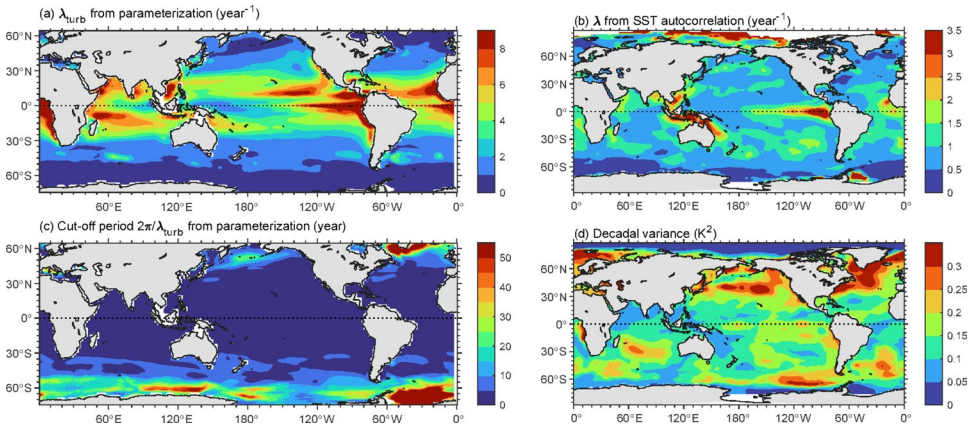

Fig. 2 **a** Ocean damping coefficient calculated from the turbulent heat flux parameterization. **b** Ocean damping coefficient calculated from the autocorrelation coefficient of the grid-point SST. **c** The cut-off period $\frac{2\pi}{\lambda_{turb}}$ from turbulent heat flux parameterization. **d** Decadal variance during 1900–2015 of global annual mean SST. The climatological period for panels **a**, **b** and **c** is 1980–2015

with temperature, $\frac{\partial e_s}{\partial T}$ is much smaller in the colder regions (Fig. 3c). Therefore, the latent heat damping is weaker in the subpolar North Atlantic, subpolar North Pacific, and the Southern Ocean, but stronger in the tropics.

In summary, in the sub-polar region of the North Atlantic, deeper mixed layers enhance heat capacity and reduce the efficacy of surface heat flux damping (Frankignoul and Hasselmann 1977; Deser et al. 2010), prolonging SST anomaly persistence. Additionally, the lower surface wind speed leads to weaker surface turbulent heat exchange, and the lower SST results in a lower latent heat damping than areas of higher temperature. These factors increase β, lower ω_c, and extend the oscillation period, thereby shaping the multidecadal variability preference of this region.

4 Spectral selectivity in a two-component coupled model with stochastic forcing

Section 3 demonstrates that stochastic forcing (e.g., synoptic weather noise) can induce amplification at low frequency bands of the response spectrum. However, this unidirectional forcing-response framework neglects bidirectional feedback between oceanic and atmospheric variability, which is a critical climate dynamic. In reality, low-frequency SST anomalies (response) modulate atmospheric circulation (forcing) through mechanisms such as surface heat fluxes and planetary wave propagation (Deser et al. 2010). Furthermore, it is suggested that stochastic forcing from the ocean can also affect the atmosphere, particularly enhancing the multidecadal variability (Tao et al. 2023). In the linear damping model, the ω_c controlled by β merely reflects the upper limit of the characteristic frequency band (approximately 50 years in the North Atlantic) to a certain extent, and cannot explain the formation of the spectral peaks—a key signature of coupled oscillations like the AMO-NAO system.

4.1 A coupled model with stochastic forcing

Here we further consider the idea of a two-dimensional coupled model with stochastic forcing. The white noise forcing is added into the coupled system to explore the behavior of its oscillation characteristics. The equations of the model are:

$$\begin{aligned} x &= x_s + \xi_x \\ y &= y_s + \xi_y \\ \frac{dx_s}{dt} &= a_x y_s + k_x \xi_y - b_x x \\ \frac{dy_s}{dt} &= a_y x_s + k_y \xi_x - b_y y \end{aligned} \tag{4}$$

where x and y represent ocean and atmosphere, x_s and y_s are the signal components of x and y, ξ_x and ξ_y are the stochastic perturbation of x and y, a_x and a_y are coupling coefficients, and b_x and b_y are damping coefficients, respectively. In this system, x and y consist of both signal and noise components. The signal components, x_s and y_s, are driven by y and x, respectively. Essentially, this interaction dynamics and the integration of stochastic forcing mirror the recharge oscillator model of El Niño-Southern Oscillation (Jin 1997; Jin et al. 2020; Zhao et al. 2024a, b).

The system can be written as:

$$\frac{d}{dt}\begin{pmatrix} x_s \\ y_s \end{pmatrix} = \begin{pmatrix} -b_x & a_x \\ a_y & -b_y \end{pmatrix}\begin{pmatrix} x_s \\ y_s \end{pmatrix} + \begin{pmatrix} -b_x & k_x \\ k_y & -b_y \end{pmatrix}\begin{pmatrix} \xi_x \\ \xi_y \end{pmatrix}.$$

Here, ξ_x (oceanic stochastic perturbation) and ξ_y (atmospheric stochastic perturbation) can be assumed physically independent of each other, as they arise from different processes such as internal turbulent mixing in the ocean and atmospheric transient vortices. Therefore, the system reduces to

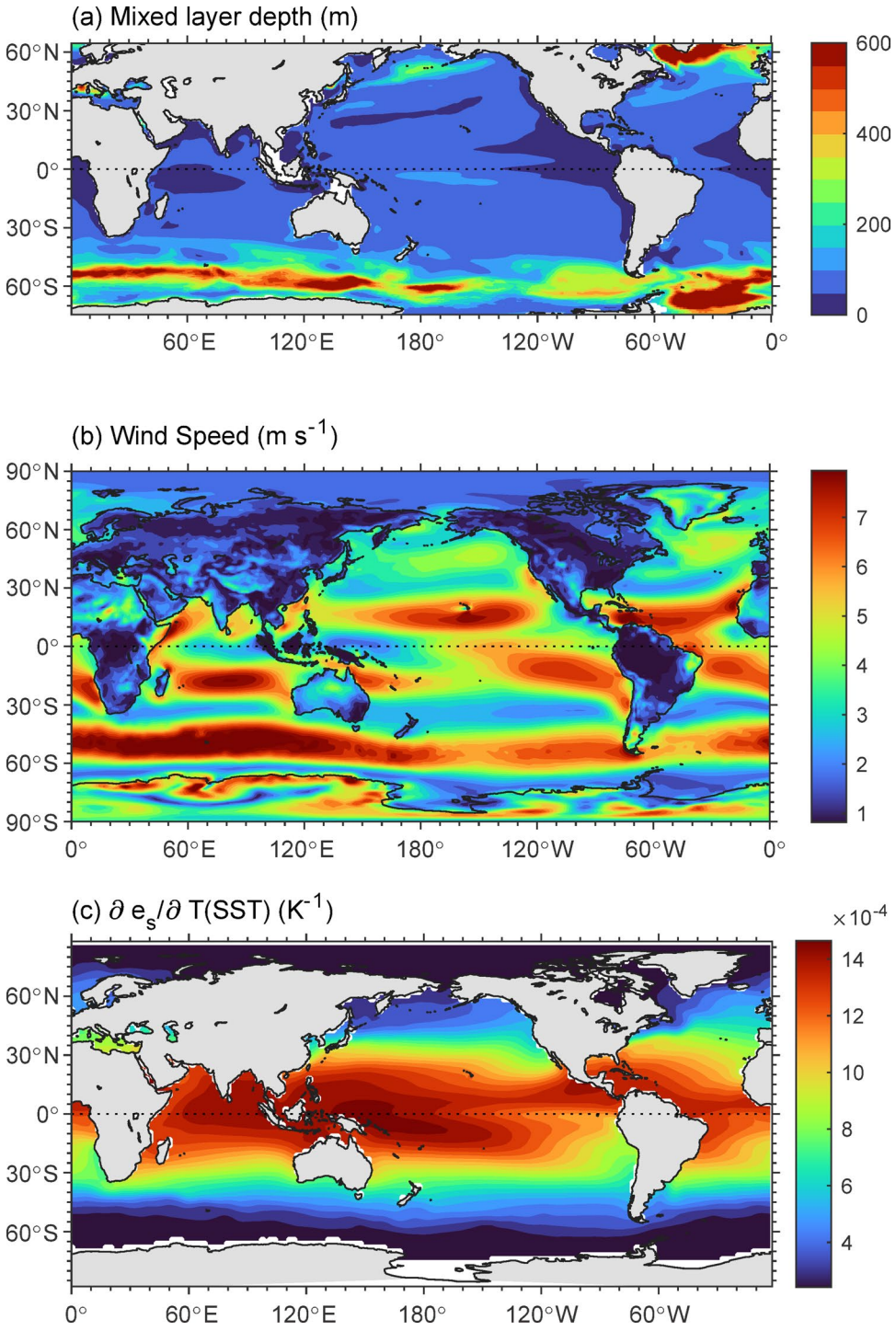

Fig. 3 Climatology of **a** mixed layer depth, **b** 10 m wind speed, and **c** $\frac{\partial e_s}{\partial T}$ at local SST for the global ocean. The climatological period for panels **a**, **b** and **c** is 1980–2015

$$\frac{d}{dt}\begin{pmatrix} x_s \\ y_s \end{pmatrix} = \boldsymbol{L}\cdot\begin{pmatrix} x_s \\ y_s \end{pmatrix} + \boldsymbol{\xi}.$$

where $\boldsymbol{L} = \begin{pmatrix} -b_x & a_x \\ a_y & -b_y \end{pmatrix}$ and $\boldsymbol{\xi}$ is the noise vector. The system's growth rate and periodicity can be analytically determined by the eigen analysis of linear operator $\boldsymbol{L}$ (Jin et al. 1997; Jin et al. 2020, and references therein). Solving $det\,(\boldsymbol{L} - \lambda \boldsymbol{I}) = 0$ yields

$$\lambda = -\frac{b_x + b_y}{2} \pm \frac{\sqrt{(b_x - b_y)^2 + 4a_x a_y}}{2}.$$

The growth rate is

$$\sigma = \frac{b_x + b_y}{2} \tag{5}$$

A necessary condition for oscillations in the system is that $(b_x - b_y)^2 + 4a_x a_y < 0$. Therefore, the product of coupling coefficients a_x and a_y is the key source of oscillation generation. When a_x and a_y are non-zero and have opposite signs, and the product is smaller than $(b_x - b_y)^2/4$, the imaginary frequency is contributed, driving the system to generate periodic oscillations. The eigenfrequency is

$$\omega = \frac{\sqrt{-(b_x - b_y)^2 - 4a_x a_y}}{2} \tag{6}$$

If the coupling disappears ($a_x = 0$ or $a_y = 0$), the system has only real roots and the oscillation ceases, degenerating into a pure attenuation or growth mode.

Following Zhao et al. (2021), one can obtain the analytical phase relationship by substituting $x_s = Xe^{\lambda t}$ and $y_s = Ye^{\lambda t}$ into the system with the stochastic terms excluded:

$$\frac{Y}{X} = \frac{\lambda + b_x}{a_x}$$

where X and Y are the complex amplitude. The argument of the ratio is exactly the phase difference ϕ_{y-x} between the x and y: $\phi_{y-x} = arg\,(\lambda + b_x) - arg\,(a_x)$. When a_1 is greater than 0:

$$\phi_{y-x} = arg\,(b_x - \sigma + i\omega) = arctan\left(\frac{2\omega}{b_x - b_y}\right)$$

The time lead corresponding to the phase difference is

$$\tau_{y-x} = \frac{\phi_{y-x}}{\omega}. \tag{7}$$

To investigate the fundamental oscillatory behavior of the coupled system, we select a set of representative parameters based on the system's intrinsic properties. For an idealized case with minimal damping ($b_x - b_y \approx 0$), the Eq. (5) simplifies to $\omega = \frac{\sqrt{-4a_x a_y}}{2}$. By setting $a_x = \frac{2\pi}{70}$ and $a_y = -\frac{2\pi}{70}$, we basically set the oscillation period $T = \frac{2\pi}{\omega} = 70$. This value is chosen to roughly align with the dominant multidecadal timescale observed in the AMO. In this preliminary setup, we treated the noise terms with the same magnitude as the coupling terms (a_x, a_y) as a default assumption: $k_x = \frac{2\pi}{70}, k_y = -\frac{2\pi}{70}$, implying that stochastic forcing and signal-based coupling have comparable influences on the system. The damping coefficients were set to small positive values ($b_x = 0.01, b_y = 0.01$) to reflect weak dissipation, which is consistent with the discussion in Sect. 3.

Long-term numerical integration with stochastic forcing reveals that the system attains a statistical equilibrium, characterized by stationary mean and variance of key variables (Fig. 4a). Experiments where the stochastic forcing and damping terms were removed separately showed that the stochastic forcing acted as an energy input to maintain the oscillation variance, while the damping term prevented the variance from diverging.

In Fig. 4b, c, the power does not increase continuously with frequency as it does in the linear model. There is a spectrum peak at a specific frequency, rather than a frequency band. For an ideal white noise forcing with a constant power spectrum, the system response is super-amplified at a specific frequency, which is determined by the parameters. The lead-lag correlation shows that the x and y lead each other, forming a coupled oscillation (Fig. 4d).

4.2 Application to the AMO-NAO oscillation and estimation of the parameters

It has been suggested that the feedback of North Atlantic Ocean onto the NAO is critical for the NAO spectrum peak at the decadal frequency band (Marshall et al. 2001; Czaja and Marshall 2000). Sun et al. (2015) introduce a model for the quasi-periodic multidecadal variability of the NAO, as follows:

$$NAO(t) \approx NAT(t)$$

$$C\frac{dAMO}{dt} = \alpha NAO - \frac{AMO}{\beta}$$

$$-NAT(t+\tau) \approx AMO(t)$$

It consists of three key dynamics: the coupling relationship between the NAO and NAT, the NAO's forcing on the AMO

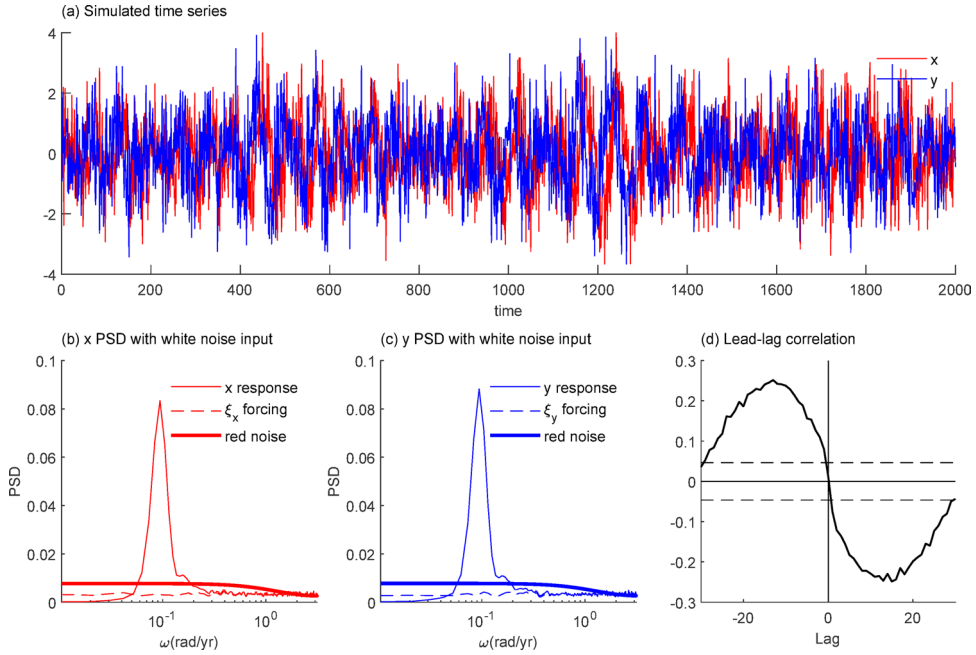

Fig. 4 Results of the stochastically forced coupled system. **a** Numerical integrated result of x and y using the parameters $a_x = k_x = \frac{2\pi}{70}$, $a_y = k_y = -\frac{2\pi}{70}$, $b_x = 0.01$, $b_y = 0.01$ for the stochastic coupled model. **b** and **c** PSD of numerical solution of stochastic coupled system with the input of artificially generated white noise. The red and blue solid lines represent the x response and y response, respectively. The red and blue dashed lines represent the white noise for the x and y, respectively. The red and blue heavy lines represent the red noise spectrum (von Storch and Zwiers 1999). The PSD was computed by Fourier-transforming the sample autocorrelation and the maximum lag $m = 300$. The spectral peaks in **b** and **c** is around 0.094 ($\approx 2\pi/67$) rad/year. **d** Lead-lag correlation between the x and the y. The dashed lines indicate the critical value at the 0.05 significance level. The positive lag denotes that the x variable leads the y variable

and the oceanic conversion from the AMO to the NAT. This leads to:

$$NAO\,(t) \approx -AMO\,(t-\tau)\,.$$

Though the model considers the oceanic feedback on atmosphere, the NAO is simply treated as a lagged correlation. Here, to consider the accumulation of ocean forcing, we construct an NAO-AMO coupled stochastic model as mentioned above:

$$\begin{aligned} AMO &= AMO_s + \xi_O \\ NAO &= NAO_s + \xi_A \\ \frac{dAMO_s}{dt} &= \frac{a_A}{c_O} NAO_s + \frac{k_A}{c_O}\xi_A - \frac{b_O}{c_O} AMO \\ \frac{dNAO_s}{dt} &= \frac{a_O}{c_A} AMO_s + \frac{k_O}{c_A}\xi_O - \frac{b_A}{c_A} NAO \end{aligned} \tag{8}$$

The physical meanings of each parameter in the model are as follows:

c_O, c_A: The heat capacity of the ocean and atmosphere.

a_A: The influence of the NAO_s on the AMO_s, including AMOC adjustments through wind-driven transport and heat fluxes (Delworth and Greatbatch 2000; Eden and Jung 2001; Álvarez-García et al. 2008).

a_O: The influence of the AMO_s on the NAO_s, including AMO's conversion to the NAT mode (Sun et al. 2015; Álvarez-García et al. 2008) and stratosphere-troposphere coupling (Omrani et al. 2022).

k_A: The influence of NAO's noise component on the AMO. It represents the synoptic scale, intraseasonal scale and interannual scale variabilities of the NAO, which are considered the non-signaling components.

k_O: The influence of AMO's noise component on the NAO. It represents the interannual scale variabilities of the AMO, which are considered the non-signaling components.

b_O: The damping rate of the AMO, including the SST damping of the surface heat flux, ocean advection and ocean entrainment dissipation.

b_A: The damping rate of the NAO, such as the Rossby wave dispersion and frictional dissipation.

The model captures the interaction of the AMO and NAO, the linear damping process, and their noise forcing effect. Note that the damping (b_O, b_A) in the coupled oscillator is no longer the purely thermodynamic damping in the linear slab-ocean model in Sect. 3 but reflects the coupled-system eigenvalues. They integrate not only surface heat flux dissipation but also the ocean dynamics (advection, entrainment and gyre-scale circulation). Therefore, these parameters are

not computed from the thermodynamic parameterization but are determined by the effective damping rates.

Estimating these parameters is a major challenge in enhancing the performance of this system. We employed a numerical least-squares optimization method to determine the parameters. The optimized parameters of the coupled model are estimated by minimizing the root mean square error (RMSE) between the model-simulated and observed annual indices of the AMO and NAO over 1854–2019.

$$RMSE = \sqrt{\frac{1}{N}\sum_{i=1}^{N}\left(AMO_{sim}\left(t_i\right) - AMO_{obs}\left(t_i\right)\right)^2} + \sqrt{\frac{1}{N}\sum_{i=1}^{N}\left(NAO_{sim}\left(t_i\right) - NAO_{obs}\left(t_i\right)\right)^2}$$

where the N is the number of years and $t_i\,(i = 1,2,\ldots,N) = 1854,1859,\ldots,2019$. The RMSE is determined by the values of the parameter set.

The initial guesses for the parameters are derived from physical and statistical methods. We use the regional average mixed layer depth h of the North Atlantic to obtain $c_O = \rho_w c_w h = 12.6\,\mathrm{W\ m^{-2}\ yr\ K^{-1}}$. The $\frac{a_A}{c_O}, \frac{a_O}{c_A}, \frac{k_A}{c_O}, \frac{k_O}{c_A}, \frac{b_O}{c_O}, \frac{b_A}{c_A}$ are estimated through simple linear regression, respectively. The time derivative terms are discretized by using forward difference and regressed onto the corresponding variables to obtain the regression coefficients as the estimated values. The signal components of the AMO and NAO are defined as the indices filtered with a 21-year Gaussian low-pass filter and the residuals are the corresponding noise components. The initial guessed parameter values obtained from the regression are $\frac{a_A}{c_O} = 0.0333\,\mathrm{K\,yr^{-1}}$ $\frac{a_O}{c_A} = -0.0307\,\mathrm{K^{-1}\ yr^{-1}}$, $\frac{k_A}{c_O} = 5.45 * 10^{-4}\,\mathrm{K\ yr^{-1}}$, $\frac{k_O}{c_A} = 0.0020\mathrm{K^{-1}\ yr^{-1}}$, $\frac{b_O}{c_O} = -0.0014\mathrm{yr^{-1}}$, $\frac{b_A}{c_A} = -0.0020\,\mathrm{yr^{-1}}$ $\frac{b_A}{c_A} = -0.0020\,\mathrm{yr^{-1}}$.

A bounded optimization approach was then employed: we sampled the parameter space within adjacent ranges (except for setting c_O to a fixed value due to a strong physical constraint) and integrated the stochastic model for each parameter set. The set of parameters that minimized the RMSE was selected as the optimal solution. This method can be viewed as a numerical least-squares optimization. The final set of determined parameters is: $c_O = 12.6\,\mathrm{W\ m^{-2}\ yr\,K^{-1}}$, $a_A = 0.76\,\mathrm{Wm^{-2}}, k_A = 0.88\,\mathrm{Wm^{-2}}, b_O = 0.029\,\mathrm{Wm^{-2}\,K^{-1}}$, $a_O/c_A = -0.09\,\mathrm{K^{-1}\,yr^{-1}}, k_O/c_A = -0.32\,\mathrm{K^{-1}\ yr^{-1}}$ and $b_A/c_A = 0.009\,\mathrm{yr^{-1}}$. Since the NAO index used here is dimensionless, c_A is a dimensionless non-independent parameter. Therefore, the parameters in the NAO equation are given combined with c_A.

Figure 5 gives the observed and numerical simulated indices using the parameters above. The coupled model successfully captures key oscillatory characteristics of the annual AMO and NAO, including their dominant multidecadal periods, phase-locked relationship (NAO leading AMO by ~ 15 years), which have been reported in previous studies (Li et al. 2013; Sun et al. 2015; Zhao et al. 2024a, b). The RMSE is 0.1443 K for the AMOI and 0.1508 std. for the NAOI.

Substituting the optimized parameters into the analytical solution (Eqs. (5)–(7) in Sect. 4.1), we obtain the growth rate, periodicity and lead-lag relationship of the system:

$$\begin{array}{l}\sigma = 0.0057\ \mathrm{year^{-1}},\\ \omega = 0.0734 \approx \frac{2\pi}{85.6}\ \mathrm{rad/year}\\ \tau_{AMO_s - NAO_s} = -18.9\ \mathrm{year}.\end{array}, \quad (9)$$

From this solution, it can be concluded that (1) this system is damped (2) the model period is about 85.6 years and (3) the NAO leading the AMO about 18.9 years. We further conduct an integral over long periods of time, with stochastic noise input. Figure 6 shows the statistical characteristics of the integral result. The system exhibits quasi-periodicity oscillations (Fig. 6a, b). The statistical characteristics are consistent with those of NAO and AMO in the observational data. The power spectrum of ocean and atmospheric variables shows peaks at low frequency (Fig. 6c). The peak of the power spectrum occurs around multidecadal timescale. The atmosphere and ocean lead each other, forming coupled oscillations (Fig. 6d). Moreover, the ocean and atmospheric components are not perfectly orthogonal. The duration of the atmospheric component leading the ocean is longer than that of the oceanic component leading the atmosphere. An asymmetric lead-lag relationship is observed with the atmosphere leading by 20–25 years and the ocean leading by ~ 20 years. When the lag is zero, they show a weak negative correlation, which is also observed in NAO-AMO lead-lag relationship (Li et al. 2013). The longer time scale of ocean response reflects the asymmetry of their physical properties.

5 Summary and discussion

This study investigates the mechanisms behind low-frequency quasi-periodic variability in the North Atlantic air-sea system. For the linear feedback model, the response of oceanic components to white noise forcing demonstrates low-pass spectrum, with significant amplification at low frequencies depending on the damping time scale β. Through parametric calculations of sensible heat and latent heat, we analyzed the spatial distribution of the damping coefficient

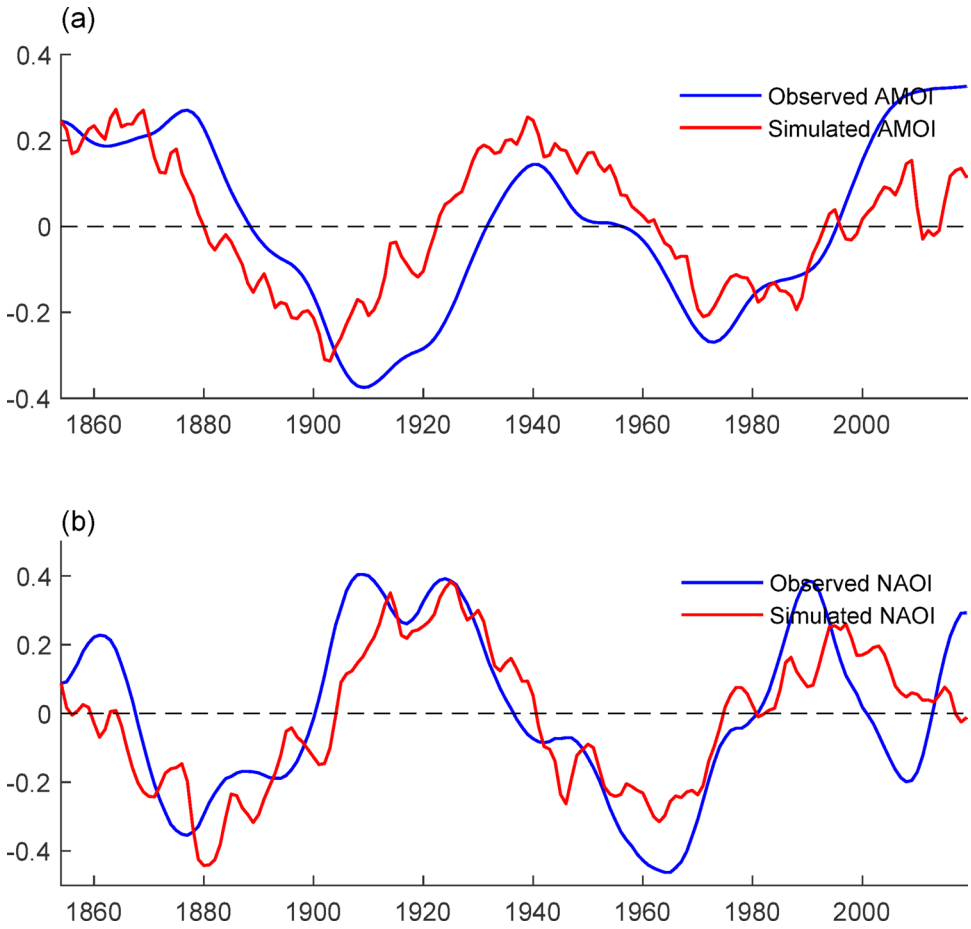

Fig. 5 Observational and simulated indices of the AMO (unit: K) and NAO (dimensionless) variability. a The observed (blue line) and simulated (red line) annual AMO indices. b As in (a), but for the NAO. Both observed indices are smoothed with a Gaussian filter using a 21-year running window

and pointed out that in the North Atlantic region, the smaller damping coefficient is an important reason for the formation of multi-decadal frequencies. This framework emphasizes the importance of mixed layer depth, surface wind speed and latent heat damping sensitivity in shaping SST variability. By incorporating stochastic forcing into a two-component coupled model, the quasi-periodic oscillations are well simulated. The model captures power spectrum peaks at low frequencies, indicating that the air-sea interactions and stochastic forcings are important to maintaining oscillatory behavior. The stochastic coupled model simulates the observed AMO and NAO indices well, matching observed characteristics. The modeled power spectrum shows peaks at multidecadal time scale.

Collectively, these results establish a mechanism that explains the spectral selectivity of air-sea coupled dynamics, as shown in Fig. 7. There are stochastic noise forcings in the ocean and atmosphere. This stochastic noise, under the influence of physical properties (such as ocean mixed layer depth), can form a response with a low frequency response. The signal components of the ocean and the atmosphere are coupled to each other. The ocean can produce a lagged response in the atmosphere lag $\sim\tau_1$ and the atmosphere, in turn, can drive the ocean with a lag$\sim\tau_2$. The ocean and atmosphere lead each other, forming a quasi-periodic coupled oscillation, whose period is$\sim 2(\tau_1+\tau_2)$. In this framework, the stochastic forcing provides the excitation, the coupling amplifies the characteristic frequency and the damping helps maintaining the steady state, which together form the spectral selectivity of the air-sea coupled system.

These frequency selectivity mechanisms describe the climate system as a spectral filter, where coupled feedbacks impose intrinsic frequency constraints rather than merely integrating stochastic inputs. We also emphasized the role of the damping coefficient, which is influenced by the physical properties and climatic characteristics of the local sea area, in shaping the frequency selectivity. It advances our understanding of low-frequency climate variability. The study underscores the importance of dynamic interactions between ocean and atmosphere providing insights into the mechanisms behind oscillatory modes like the AMO and NAO. While studies have predominantly attributed multidecadal periodicity to AMOC's advective timescales (Sun et al. 2015; Li et al. 2025), our results reveal an alternative local-scale mechanism governed by mixed layer thermal inertia and surface heat damping that actively shapes spectral selectivity. This provides perspective to assess future AMO changes under evolving ocean stratification.

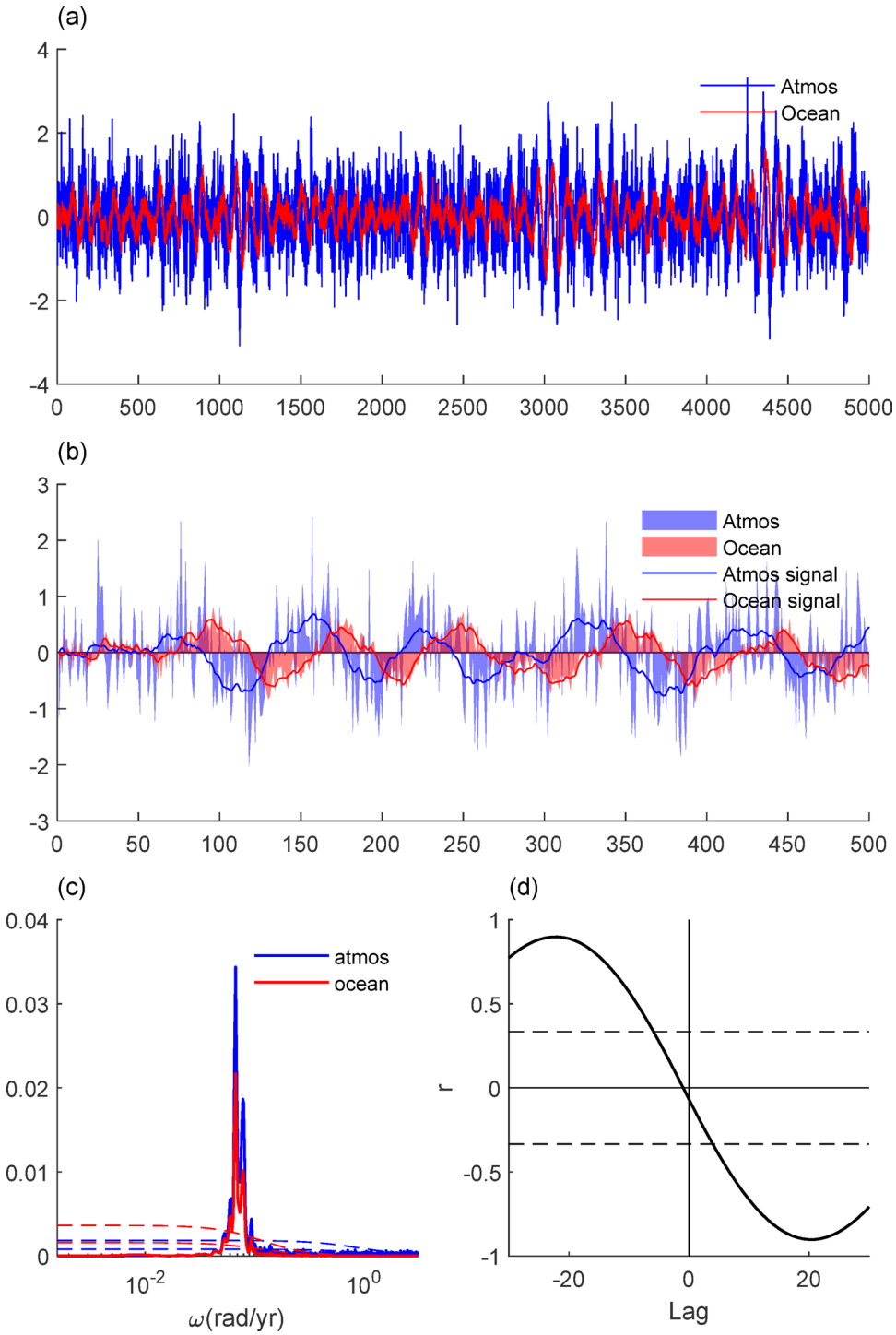

Fig. 6 Stochastic coupled variability across centennial to millennial simulations. **a** Numerical solution of 5000 years of the stochastic coupled system using the parameters from the observation. The initial values of signal components are set to zero. The stochastic forcing is set to white noise. The blue and red lines denote the atmosphere variable and oceanic variable, respectively. **b** Same as **a**, but for the first 500 years. The signal components are plotted to illustrate the oscillation. **c** PSD of the oceanic (red solid line) and atmospheric (blue solid line) variables in the stochastic coupled system. The red (blue) dashed lines are the PSD of red noise and its critical value at 0.05 significance level for the oceanic (atmospheric) variable (von Storch and Zwiers 1999). The PSD was computed by Fourier-transforming the sample autocorrelation and the maximum lag $m = 2000$. The spectral peaks in **c** are around 0.06–0.07 ($\approx 2\pi/105 - 2\pi/90$) rad/year. **d** Lead-lag correlation between the signal components of the atmospheric and oceanic variables. The positive lag denotes that the ocean variable leads the atmosphere variable. The black dashed lines indicate the 0.05 significance level

The findings have implications beyond the North Atlantic, offering an insight for analyzing coupled variability in other ocean–atmosphere systems.

Our analytical framework offers a powerful process-oriented tool for evaluating general circulation models by deriving parameters from observational data and comparing them against model-simulated NAO and AMO. This method enables diagnosis of biases such as in ocean–atmosphere coupling strength (a_O) or damping timescales (c_O/b_O) which often underlie errors in simulated multidecadal variability. By moving beyond mere spectral comparisons to specific processes, our approach provides feedback for refining parameterizations (e.g., surface flux exchanges or oceanic mixing), thereby supporting the development of more reliable climate projections.

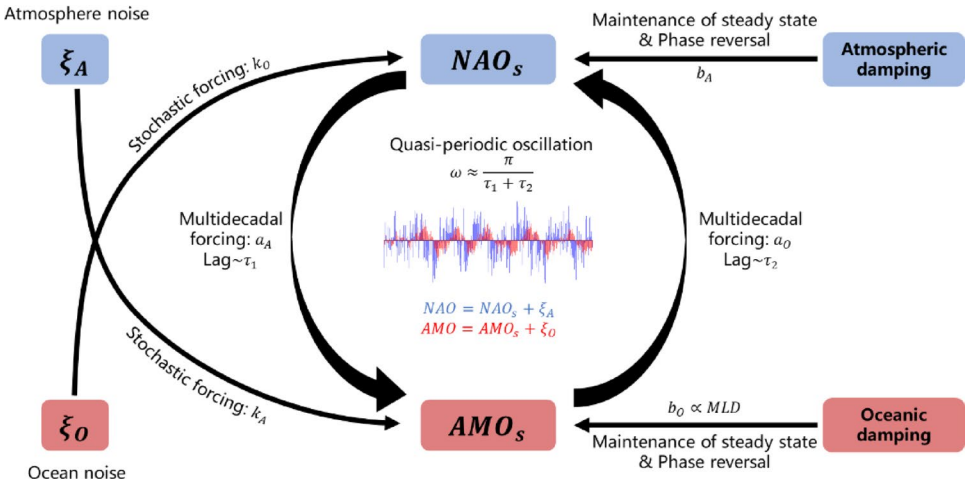

Fig. 7 Schematic diagram about the mechanism of the spectral selectivity phenomenon in the air-sea coupled system

While the slab-ocean model successfully captures the key spectral characteristics of the AMO variability, it only parameterizes the net turbulent heat flux damping effect. In reality, the effective oceanic damping is not solely controlled by mixed-layer thermodynamics but also involves important contributions from ocean dynamical processes (Zhang et al. 2019). These include lateral heat advection by mean currents and ocean gyres, entrainment due to wind-driven mixing, and the integrated effect of mesoscale eddies. These processes can modulate the persistence of SST anomalies and thus the perceived damping timescale (Gunnarson et al. 2024). Our conceptual coupled model aggregates these effects into a single effective damping parameter, and future studies are needed to disentangle their relative contributions.

Although the results reproduce observed variability, its validation is restricted to case study in the North Atlantic. The assumption of white noise forcing overlooks potential atmospheric noises with other frequency or memory characteristic that could further influence variability. Future studies could extend to other climate modes, such as the Pacific Decadal Oscillation, and explore nonlinear feedbacks and more complex stochastic forcings.

Acknowledgements This research was jointly supported by the National Natural Science Foundation of China (NSFC) Project (42130607), Laoshan Laboratory (No.LSKJ202202600), Shandong Natural Science Foundation Project (ZR2019ZD12) and Fundamental Research Funds for the Central Universities (202242001).

Author contributions All authors contributed to the study conception and design. Model development, numerical simulations, and data analysis were performed by Hongyuan Zhao. The first draft of the manuscript was written by Hongyuan Zhao and all authors critically revised subsequent versions. Jianping Li supervised the theoretical framework development and validation. Both authors reviewed and approved the final manuscript.

Funding This research was jointly supported by the National Natural Science Foundation of China (NSFC) Project (42130607), Laoshan Laboratory (No.LSKJ202202600), Shandong Natural Science Foundation Project (ZR2019ZD12) and Fundamental Research Funds for the Central Universities (202242001).

Data availability The datasets analyzed during this study are publicly available from the following repositories: Sea surface temperature data: NOAA Extended Reconstructed SST Version 5 (ERSSTv5). https://www.ncei.noaa.gov/products/extended-reconstructed-sst. Mixed layer depth data: NCEP Global Ocean Data Assimilation System (GODAS). https://psl.noaa.gov/data/gridded/data.godas.html. 10 m wind data: NCEP-NCAR Reanalysis 1. https://psl.noaa.gov/data/gridded/data.ncep.reanalysis.html. Sea level pressure data: HadSLP2. https://www.metoffice.gov.uk/hadobs/hadslp2.

Declarations

Competing interests The authors have no relevant financial or non-financial interests to disclose.

References

Tao L, Sun X, Yang X-Q, Fang J, Zhang Z-Q (2023) Effect of oceanic stochastic forcing on wintertime atmospheric decadal variability over midlatitude North Pacific. J Geophys Res Atmos 128:e2022JD037594. https://doi.org/10.1029/2022JD037594}

Allan R, Ansell T (2006) A new globally complete monthly historical gridded mean sea level pressure dataset (HadSLP2): 1850–2004. J Climate 19:5816–5842. https://doi.org/10.1175/JCLI3937.1

Álvarez-García F, Latif M, Biastoch A (2008) On multidecadal and quasi-decadal North Atlantic variability. J Climate 21:3433–3452. https://doi.org/10.1175/2007JCLI1800.1

Cane MA, Clement AC, Murphy LN, Bellomo K (2017) Low-pass filtering, heat flux, and Atlantic multidecadal variability. J Climate 30:7529–7553. https://doi.org/10.1175/JCLI-D-16-0810.1

Clement A, Bellomo K, Murphy LN et al (2015) The Atlantic multidecadal oscillation without a role for ocean circulation. Science 350:320–324. https://doi.org/10.1126/science.aab398

Czaja A, Marshall J (2000) On the interpretation of AGCMs response to prescribed time-varying SST anomalies. Geophys Res Lett 27:1927–1930. https://doi.org/10.1029/1999GL011322

Delworth TL, Greatbatch RJ (2000) Multidecadal thermohaline circulation variability driven by atmospheric surface flux forcing. J Climate 13:1481–1495. https://doi.org/10.1175/1520-0442(2000)013%3c1481:MTCVDB%3e2.0.CO;2

Delworth TL, Zeng F, Zhang L et al (2017) The central role of ocean dynamics in connecting the North Atlantic oscillation to the

extratropical component of the Atlantic multidecadal oscillation. J Climate 30:3789–3805. https://doi.org/10.1175/JCLI-D-16-0358.1
Derber JC, Rosati A (1989) A global oceanic data assimilation system. J Phys Oceanogr 19:1333–1347. https://doi.org/10.1175/1520-0485(1989)019%3c1333:AGODAS%3e2.0.CO;2
Deser C, Alexander MA, Xie S et al (2010) Sea surface temperature variability: patterns and mechanisms. Annu Rev Mar Sci 2:115–143. https://doi.org/10.1146/annurev-marine-120408-151453
Eden C, Jung T (2001) North Atlantic interdecadal variability: oceanic response to the North Atlantic oscillation (1865–1997). J Climate 14:676–691. https://doi.org/10.1175/1520-0442(2001)014%3c0676:NAIVOR%3e2.0.CO;2
Frankcombe LM, Dijkstra HA, von der Heydt A (2008) Sub-surface signatures of the Atlantic Multidecadal Oscillation. Geophys Res Lett 35:L19602. https://doi.org/10.1029/2008GL034989
Frankcombe LM, Dijkstra HA, von der Heydt A (2009) Noise-induced multidecadal variability in the North Atlantic: excitation of normal modes. J Phys Oceanogr 39:220–233. https://doi.org/10.1175/2008JPO3951.1
Frankignoul C (1985) Sea surface temperature anomalies, planetary waves, and air-sea feedback in the middle latitudes. Rev Geophys 23:357–390. https://doi.org/10.1029/RG023i004p00357
Frankignoul C, Hasselmann K (1977) Stochastic climate models, Part II application to sea-surface temperature anomalies and thermocline variability. Tellus 29:289–305. https://doi.org/10.3402/tellusa.v29i4.11362
Frankignoul C, Czaja A, L'Heveder B (1998) Air-sea feedback in the North Atlantic and surface boundary conditions for ocean models. J Climate 11:2310–2324. https://doi.org/10.1175/1520-0442(1998)011%3c2310:ASFITN%3e2.0.CO;2
Gunnarson JL, Stuecker MF, Zhao S (2024) Drivers of future extratropical sea surface temperature variability changes in the North Pacific. NPJ Clim Atmos Sci 7:164. https://doi.org/10.1038/s41612-024-00702-5
Hasselmann K (1976) Stochastic climate models: Part I. theory. Tellus 28:473–485. https://doi.org/10.3402/tellusa.v28i6.11316
Higham DJ (2001) An algorithmic introduction to numerical simulation of stochastic differential equations. SIAM Rev 43:525–546. https://doi.org/10.1137/S0036144500378302
Huang B, Thorne PW, Banzon VF et al (2017) Extended Reconstructed Sea Surface Temperature, Version 5 (ERSSTv5): upgrades, validations, and intercomparisons. J Climate 30:8179–8205. https://doi.org/10.1175/JCLI-D-16-0836.1
Jin F (1997) An equatorial ocean recharge paradigm for ENSO. Part I: conceptual model. J Atmos Sci 54:811–829. https://doi.org/10.1175/1520-0469(1997)054%3c0811:AEORPF%3e2.0.CO;2
Jin FF, Chen HC, Zhao S, Hayashi M, Karamperidou C, Stuecker MF, Xie R, Geng L (2020) Simple ENSO models. In: McPhaden MJ, Santoso A, Cai W (eds) El Niño Southern Oscillation in a Changing Climate. https://doi.org/10.1002/9781119548164.ch6
Kalnay E, Kanamitsu M, Kistler R et al (1996) The NCEP/NCAR 40-Year Reanalysis Project. B Am Meteorol Soc 77:437–472. https://doi.org/10.1175/1520-0477(1996)077%3c0437:TNYRP%3e2.0.CO;2
Kerr RA (2000) A North Atlantic climate pacemaker for the centuries. Science 288:1984–1986. https://doi.org/10.1126/science.288.5473.1984
Li JP, Wang JXL (2003) A new North Atlantic Oscillation index and its variability. Adv Atmos Sci 20:661–676. https://doi.org/10.1007/BF02915394
Li JP, Sun C, Jin FF (2013) NAO implicated as a predictor of Northern Hemisphere mean temperature multidecadal variability. Geophys Res Lett 40:5497–5502. https://doi.org/10.1002/2016JD025979
Li S, Wu L, Wang Y et al (2025) Intensified Atlantic multidecadal variability in a warming climate. Nat Clim Change 15:293–300. https://doi.org/10.1038/s41558-025-02252-x
Liu Z (2012) Dynamics of interdecadal climate variability: a historical perspective. J Climate 25:1963–1995. https://doi.org/10.1175/2011JCLI3980.1
Lozier MS (2012) Overturning in the North Atlantic. Annu Rev Mar Sci 4:291–315. https://doi.org/10.1146/annurev-marine-120710-100740
Marshall J, Johnson H, Goodman J (2001) A study of the interaction of the North Atlantic Oscillation with Ocean circulation. J Climate 14:1399–1421. https://doi.org/10.1175/1520-0442(2001)014%3c1399:ASOTIO%3e2.0.CO;2
Omrani NE, Keenlyside N, Matthes K et al (2022) Coupled stratosphere-troposphere-Atlantic multidecadal oscillation and its importance for near-future climate projection. NPJ Clim Atmos Sci 5:59. https://doi.org/10.1038/s41612-022-00275-1
Pivotti V, Anderson BT (2021) Transition between forced and oscillatory ENSO behavior over the last century. J Geophys Res Atmos 126:e2020JD034116. https://doi.org/10.1029/2020JD034116
Schlesinger ME, Ramankutty N (1994) An oscillation in the global climate system of period 65–70 years. Nature 367:723–726. https://doi.org/10.1038/367723a0
Sun C, Li JP, Jin FF (2015) A delayed oscillator model for the quasi periodic multidecadal variability of the NAO. Clim Dyn 45:2083–2099. https://doi.org/10.1007/s00382-014-2459-z
von Storch H, Zwiers FW (1999) Statistical analysis in climate research. Cambridge University Press, Cambridge. https://doi.org/10.1017/CBO9780511612336
Wei X, Zhang R (2022) A simple conceptual model for the self-sustained multidecadal AMOC variability. Geophys Res Lett 49:e2022GL099800. https://doi.org/10.1029/2022GL099800
Zhang R, Sutton R, Danabasoglu G, Delworth TL, Kim WM, Robson J, Yeager SG (2016) Comment on "The Atlantic Multidecadal Oscillation without a role for ocean circulation." Science 352:1527–1527. https://doi.org/10.1126/science.aaf1660
Zhang R, Sutton R, Danabasoglu G et al (2019) A review of the role of the Atlantic Meridional Overturning Circulation in Atlantic Multidecadal Variability and associated climate impacts. Rev Geophys 57:316–375. https://doi.org/10.1029/2019RG000644
Zhao S, Stuecker MF, Jin FF et al (2020) Improved predictability of the Indian Ocean Dipole using a stochastic dynamical model compared to the North American Multimodel Ensemble Forecast. Weather Forecast 35:379–399. https://doi.org/10.1029/2019GL084196
Zhao S, Jin FF, Stuecker MF (2021) Understanding lead times of warm water volumes to ENSO sea surface temperature anomalies. Geophys Res Lett 48:e2021GL094366. https://doi.org/10.1029/2021GL094366
Zhao H, Li JP, Liu Y et al (2024a) Multidecadal variability from ocean to atmosphere in the North Atlantic: perturbation potential energy as the bridge. J Climate 37:5187–5206. https://doi.org/10.1175/JCLI-D-24-0025.1
Zhao S, Jin FF, Stuecker MF et al (2024b) Explainable El Niño predictability from climate mode interactions. Nature 630:891–898. https://doi.org/10.1038/s41586-024-07534-6

Publisher's Note Springer Nature remains neutral with regard to jurisdictional claims in published maps and institutional affiliations.

Springer Nature or its licensor (e.g. a society or other partner) holds exclusive rights to this article under a publishing agreement with the author(s) or other rightsholder(s); author self-archiving of the accepted manuscript version of this article is solely governed by the terms of such publishing agreement and applicable law.